Ammonium-controlled nano-fibrillar boehmite synthesis through electrolysis from aluminate solutions

Jean-Luc Trompette, Laurent Cassayre, Sébastien Teychené

Trends in Physical Chemistry
Vol. 18, 2018

Original Article

Ammonium-controlled nano-fibrillar boehmite synthesis through electrolysis from aluminate solutions

Jean-Luc Trompette*, Laurent Cassayre and Sébastien Teychené

Laboratoire de Génie Chimique UMR 5503, Université de Toulouse, CNRS, 4 allée Emile Monso, 31432 Toulouse Cedex 4, France.

ABSTRACT

The synthesis of nano-fibrillar boehmite through electrolysis with a sacrificial aluminum anode in the presence of 0.1 mol/L sulfate electrolyte solutions at initial pH 9 and at 60 °C was carried out. The beneficial use of ammonium salt has allowed maintaining pH at a level compatible for the exclusive formation of boehmite during electrolysis from aluminate solutions. According to the experimental results and analyses inferred from X-ray diffraction pattern (XRD), transmission electron microscopy (TEM) and energy dispersive spectroscopy (EDS) characterizations, the mechanism of synthesis was described.

KEYWORDS: boehmite, nanofibrillar, electrolysis, aluminate, ammonium.

INTRODUCTION

The aluminum oxihydroxide boehmite, γ-AlOOH, is used as adsorbents and catalysts; however it is widely employed as a key precursor to synthesize gamma alumina, γ-Al_2O_3. This transition alumina allows accessing to many other allotropic phases of alumina through controlled temperature treatments [1-3]. Moreover, γ-Al_2O_3 is extensively used as an industrial catalyst carrier in the field of petrochemicals and fine chemicals [4, 5]. Upon calcination at around 500 °C, boehmite undergoes a topotactic transformation into gamma alumina where the size and the morphology are conserved:

$$2\gamma\text{-}AlOOH \rightarrow \gamma\text{-}Al_2O_3 + H_2O \quad (1)$$

In many engineering applications the textural and surface properties of γ-Al_2O_3 (shape, surface area, pore size distribution, electric charge) play a crucial role so that the formation of nanofiber or one-dimensional (1D) structure of γ-AlOOH has been sought after. Numerous experimental investigations have been undertaken for many years to synthesize boehmite fibers using different methods, such as precipitation reactions [6-11], hydrothermal routes [12-21], sol-gel techniques [22-25], and other approaches like laser ablation [26], and steam-assisted method [27]. Nevertheless specific conditions have to be applied to avoid the concomitant formation of other types of hydrated alumina phases [28-31], i.e. aluminum trihydroxides, such as bayerite (α-$Al(OH)_3$), and/or nordstrandite (β-$Al(OH)_3$) and/or gibbsite (γ-$Al(OH)_3$). In the case of the precipitation method for instance, pH-temperature maps have been established to define the existence domains of boehmite [3, 4, 6]. Whatever the method, important parameters such as pH [16, 18, 32], temperature [14, 29, 33], solution composition [34-38] and ageing [39-41], were found to influence the size and the morphology of boehmite crystallites. This was presumed to be in close relation with the solid-liquid interfacial energies of the implied crystallite facets [42, 43].

Although electrocoagulation is a widespread electrolysis technique for the *in situ* treatment of aqueous effluents with the aid of metal electrodes such as aluminum [44, 45], the synthesis of

*Corresponding author: jeanluc.trompette@ensiacet.fr

hydrated alumina samples through electrolysis from aluminum plates has been scarcely reported in the literature. An aluminum anode was used for electrolysis of an aqueous acetic acid solution [46]. A greyish gel was recovered and heated in boiling water to obtain a concentrated white sol of lath-like crystals of boehmite. Later, electrolysis of diluted NaCl solutions with a pair of aluminum electrodes were performed by applying variable electrical potentials [47]. Above 30 V fibrous boehmite was predominantly, but not exclusively, formed while below 20 V a mixture of bayerite and boehmite was obtained. Hydrated alumina samples have also been synthesized from various electrolyte solutions at the original pH [48, 49] but without any anticipated control of the produced phases. The resulting dried samples were employed as adsorbents for the removal of pollutants in aqueous media.

In the present study, electrolysis experiments with an aluminum anode were performed at initial pH = 9 and temperature at 60 °C in the presence of sulfate electrolyte as a morphology-directing agent. Indeed, previous precipitation studies have inspired the choice of these experimental conditions [7, 11] and the nature of the used salt [5, 18] since they allowed boehmite formation with a nano-fibrillar structure of desired properties. These conditions match effectively the schematic pH-temperature diagram of hydrated alumina phases [3], see Figure 1. Although the boehmite formation domain is restricted at ambient temperature it becomes more favorable for a wider range of pH above 60 °C. It has been already emphasized that an alkaline medium is preferable for fast boehmite formation since the conversion from amorphous phase to boehmite is faster than the conversion of boehmite to aluminum trihydroxide phases [39]. Moreover, in light of previous electrocoagulation studies with aluminum plates, the use of ammonium salts has been investigated since it was shown to play a beneficial role on pH regulation through a buffering effect during electrolysis [50, 51].

In this work, the conditions and the underlying mechanism allowing exclusive formation of nano-fibrillar boehmite through electrolysis from aluminate solutions have been studied. The samples were analyzed through XRD, TEM, EDS and Brunauer–Emmet–Teller (BET) characterizations.

MATERIALS AND METHODS

Sodium sulfate (Na_2SO_4) and ammonium sulfate ($(NH_4)_2SO_4$) were provided by Sigma-Aldrich (France). Deionized water was taken as a solvent to prepare 100 mL of the electrolytic solution at

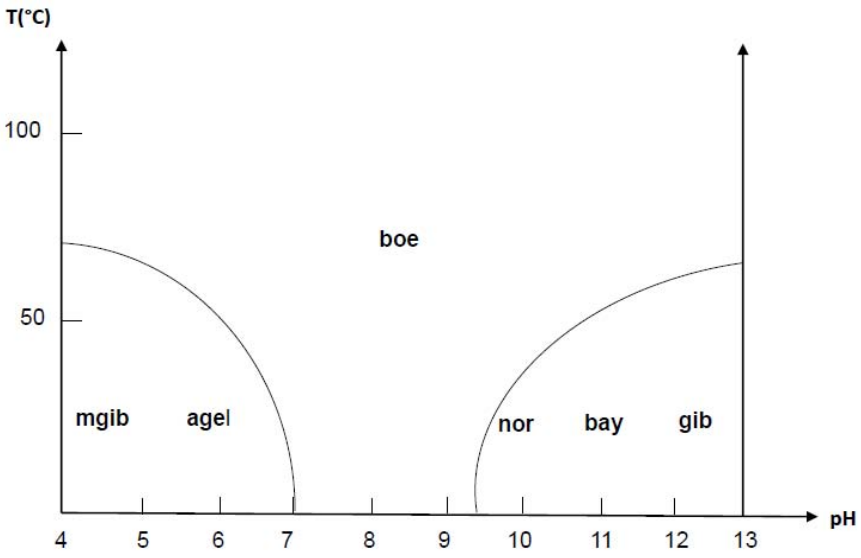

Figure 1. Schematic pH-temperature diagram of hydrated alumina phases (boe: boehmite; nor: nordstrandite; bay: bayerite; gib: gibbsite; mgib: microcrystalline gibbsite; agel: amorphous gel).

0.1 mol/L concentration. Sulfuric acid H_2SO_4 (98%, w/w) was from Prolabo (France).

Aluminum plates with a rectangular shape (7 cm × 2.5 cm) were cut from a commercial sheet of 1050 aluminum alloy (chemical composition in per cent weight: 99.5% Al, < 0.40% Fe, < 0.25% Si, < 0.05% Cu) with a thickness of 0.5 mm. Before the experiment, the aluminum plate was degreased with acetone.

The non-deaerated electrolytic solution was placed into a double-jacked reactor and it was thermostated at 60 °C through a regulator bath (Lauda Eco Silver). Aliquots of a concentrated sodium hydroxide (NaOH) solution were then added to adjust the electrolytic solution at pH 9 before electrolysis. The electrochemical set up was comprised of an aluminum plate as the anode and a platinum plate as the cathode. The anode-cathode distance was fixed at 2 cm and the electrodes were immersed at 3.5 cm depth in 100 mL of the thermostated electrolytic solution (the active geometric area of the anode was 17.85 cm²). Electrolysis experiments were performed for 2 hours by imposing a 0.9 A current intensity through a DC power supply (Convergie Fontaine, 1 A - 400 V). The solution was gently agitated with a magnetic stirrer. An electronic pH-meter (Eutech Instruments) was used for the measurements.

After electrolysis, the obtained white slurry was recovered and maintained under magnetic agitation to reach ambient temperature. It was subsequently centrifuged for 10 minutes at 12,000 rpm and the conductivity of the resulting supernatant was measured. As long as the conductivity was greater than 100 µS/cm the collected paste was rinsed with 100 mL of deionized water under magnetic agitation before a new centrifugation step. The resulting washed paste was oven-dried at 95 °C overnight and it was further manually grinded to obtain a fine powder for analysis. All experiments were repeated twice.

The X-ray diffraction patterns (XRD) of dried powders were recorded at room temperature with Cu Kα radiation (λ = 1.5418 Å) of a Bruker Advance D8 diffractometer. The intensity data were measured between 5° to 120° with a 0.02 step length. Boehmite and other hydrated alumina phases were identified through comparison of the position of the recorded peaks with those of standard references from Joint Committee on Powder Diffraction Standards (JCPDS) [2].

Micrographs from transmission electron microscopy (TEM) were obtained using a JEOL JEM 1400 model operating at 120 kV. A small amount of powder was dispersed in ethanol using an ultrasound bath. A copper grid (coated with a thin adhesive polymer film) was then soaked into this dispersion and it was left for drying in air before analysis.

Element analysis by energy dispersive spectroscopy (EDS) was performed using a JEOL JSM 7100F model operating at 10 kV accelerating voltage.

Nitrogen adsorption-desorption isotherms were measured at 77 K using a Belsorp model (Bel Japan, Inc.) and assuming a 0.164 nm² nitrogen molecule cross section. The specific surface area was determined by the BET method and the pore size distribution was determined from the desorption branch of the isotherm by the BJH (Barrett–Joyner–Halenda) method.

RESULTS AND DISCUSSION

When electrolysis starts, bubbles appear instantaneously on both electrodes although fewer bubbles are electrogenerated at the anode surface. After some minutes, tiny insoluble aggregates are captured by ascending bubbles so that a loose foam is created at the solution surface. Further, the electrolyte becomes increasingly turbid owing to the formation of larger particle aggregates. After about 40-45 minutes, a whitish color develops in suspension (the electrodes are no longer visible). When electrolysis and agitation are stopped, the white slurry separates and a consequent precipitate is formed. The characteristic smell of ammonia (NH_3) is detected when electrolysis is performed with the ammonium salt. This was confirmed through the Nessler's reagent [50].

In a typical electrolysis experiment the corresponding weight loss of the aluminum anode is $\Delta m = 0.487$ g, so that the experimental mole number of dissolved aluminum is 0.018 moles. After the centrifugation/ rinsing and drying/grinding steps the amount of hydrated alumina sample was between 1.2 to 1.3 g.

According to the Faraday's law, the maximal mole number of aluminum cations released from the anode as a function of time is:

$$n_{Al} = \frac{it}{zF} = 3.109 \times 10^{-6} . t \quad (2)$$

where i is the applied current intensity (0.9 A) during time electrolysis t (in seconds), z is the valence of aluminum cation (z = 3) and F is the Faraday constant (96500 C/mol). The maximal amount of dissolved aluminum corresponding to 2 hours of electrolysis is n_{Al} = 0.022 moles. Since mass balance indicated an average 0.018 moles of dissolved aluminum, it reveals that the major anodic reaction is Al dissolution (82% of the current), while water oxidation into O_2(g) is secondary.

As evidenced in Figure 2, pH variation during electrolysis is intimately related to the electrolyte composition and this may influence the nature of hydrated alumina phases in accordance with Figure 1. With sodium sulfate (□), pH increases continuously from 9 and stabilizes around 11 after 1 hour. With ammonium sulfate (♦), pH starts to decrease after 15 minutes and reaches a final value between 7.5 to 8.

Once the powders were obtained after rinsing and drying, X-ray diffraction analysis was performed to determine the nature of the hydrated alumina phases, see Table 1.

The XRD analyses for $(NH_4)_2SO_4$ and Na_2SO_4 electrolytes are shown in Figure 3 and Figure 4, respectively. Boehmite is produced with both electrolytes; however boehmite is the sole phase obtained in the case of the ammonium salt. With the sodium salt (Figure 4), boehmite is mixed with aluminum trihydroxide phases, i.e. bayerite and gibbsite, where the presence of supplementary characteristic peaks is evidenced when compared to Figure 3.

TEM observations of the powder obtained in the presence of $(NH_4)_2SO_4$ and Na_2SO_4 electrolytes are shown in Figures 5 and 6, respectively.

As expected from precipitation studies within the same temperature and pH conditions, boehmite exhibits a nano-fibrillar structure. The TEM image at higher magnification in Figure 5 suggests fibrils resulting from lateral alignment of boehmite crystallites. As bundles of nanofibers are present in each case (since boehmite is formed), the presence of large objects in Figure 6 is ascribed to

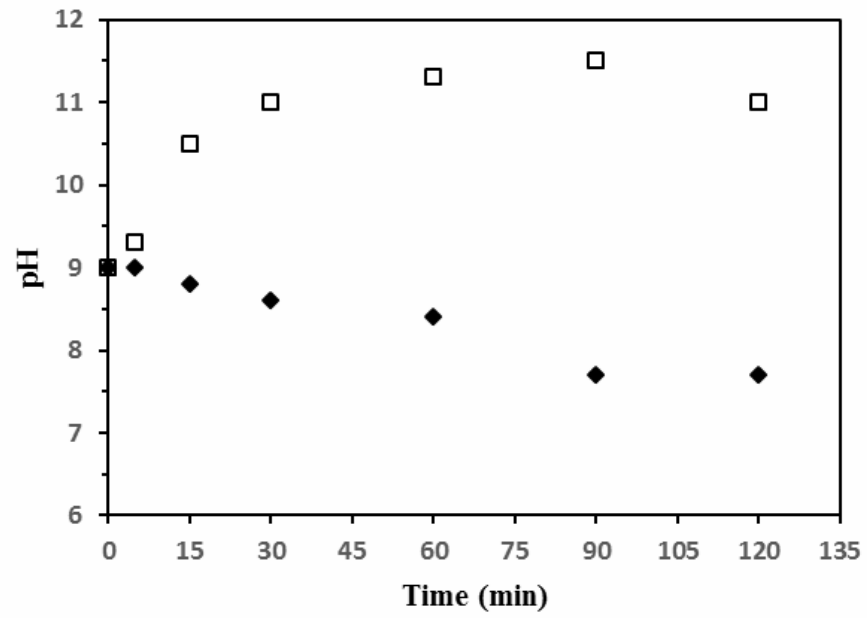

Figure 2. Variation of the solution pH as a function of electrolysis duration: 0.1 mol/L Na_2SO_4 (□), 0.1 mol/L $(NH_4)_2SO_4$ (♦).

Table 1. Phase identification (XRD) of hydrated alumina samples and atomic percentage of sulfur (EDS) in hydrated alumina sample as a function of the sulfate salt.

Electrolyte	XRD analysis	EDS analysis (% S atom)
$(NH_4)_2SO_4$	boehmite	1.0 S
Na_2SO_4	boehmite + bayerite + gibbsite	0.0 S

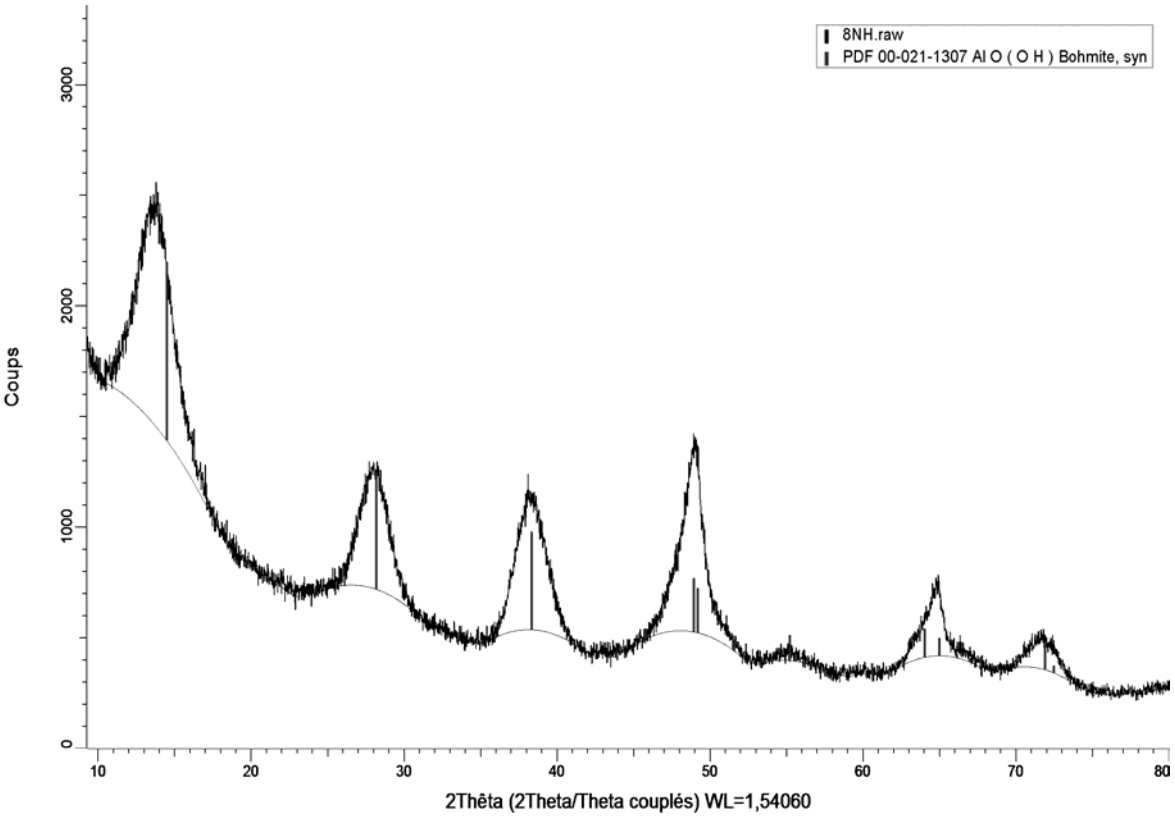

Figure 3. XRD analysis of the powder resulting from electrolysis with 0.1 mol/L $(NH_4)_2SO_4$.

aluminum trihydroxide phases where the characteristic conical or hourglass shape of bayerite particles is notably observed [1, 2].

As the isoelectric point (iep) of boehmite has been reported to be around pH 9 [52], it is expected that incipient boehmite crystallites should not experience strong electrostatic repulsion from one another. Moreover, at the 0.1 mol/L electrolyte concentration the corresponding Debye length, κ^{-1}, is significantly lowered so that the screening of the surface charges is highly effective [53]. At 60 °C in aqueous media: $\kappa^{-1} = \frac{0.325}{\sqrt{I}}$ ≈1 nm (*I* is the ionic strength: $I = \frac{1}{2}\sum_i c_i . z_i^2$ where c_i and z_i are the molar concentration and the valence of ion i, respectively). Within these conditions attractive van der Waals forces are largely dominant so that aggregation of boehmite nanoparticles is promoted leading to structures with an open porosity [53].

Nano-fibrillar boehmite samples were characterized by nitrogen gas adsorption-desorption experiments, as illustrated by case A in Figure 7, where the adsorbed volume (V) is plotted as a function of the relative pressure (p/p_0). The BET specific surface area was about 310 m²/g. The pore size

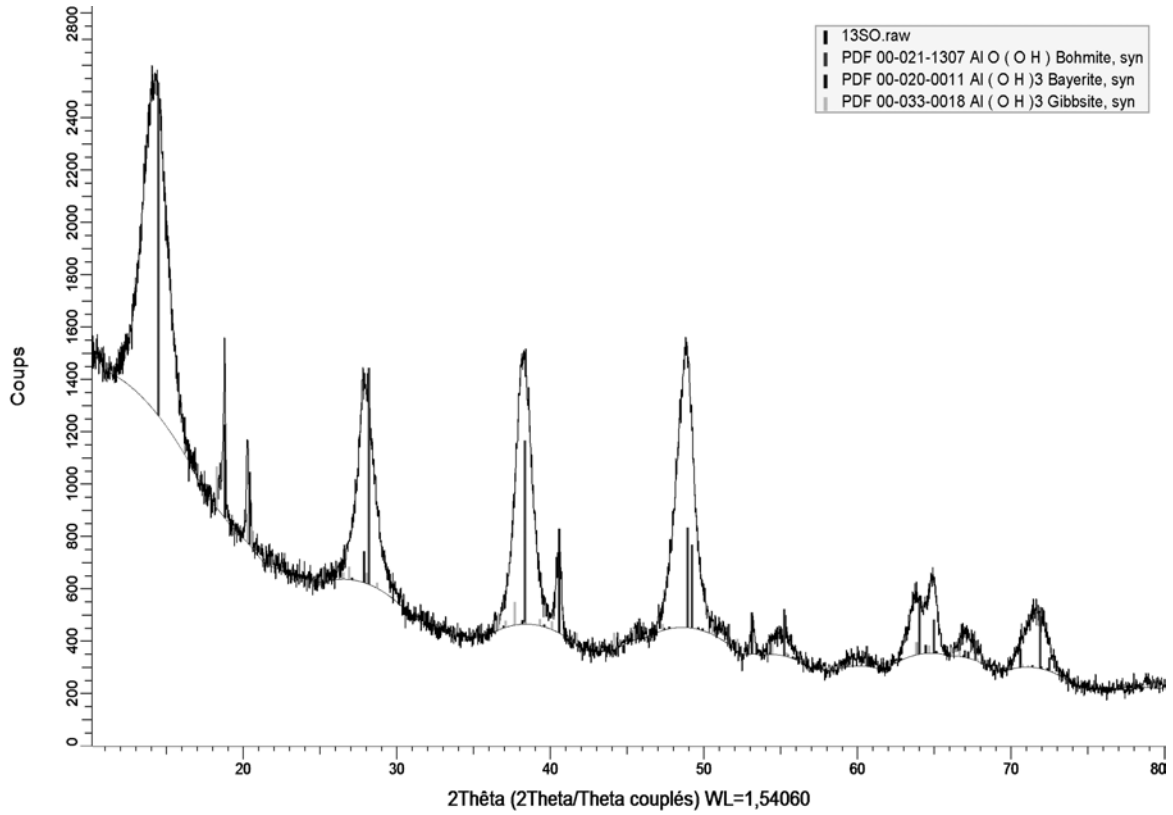

Figure 4. XRD analysis of the powder resulting from electrolysis with 0.1 mol/L Na_2SO_4.

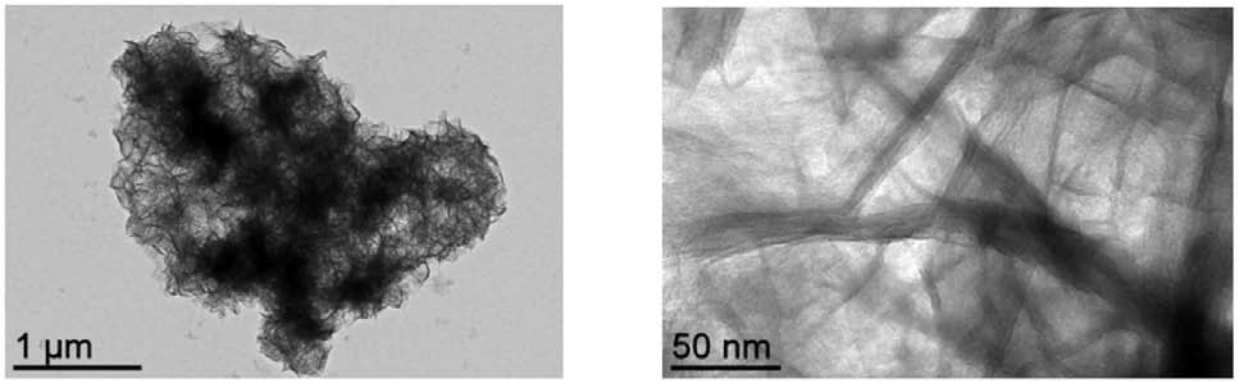

Figure 5. TEM images of boehmite sample resulting from electrolysis with 0.1 mol/L $(NH_4)_2SO_4$.

distribution was determined through the BJH method using the isotherm desorption data by plotting dV_p/dD_p (desorption pore volume V_p) versus pore diameter (D_p), see case B in Figure 7. The mean pore diameter and the pore volume were 4.2 nm and 0.869 cm^3/g, respectively. These results are comparable with those of boehmite samples obtained through the precipitation method within the same conditions [7].

In order to understand the role of the electrolyte on the evolution of the solution pH, the main chemical and electrochemical reactions were

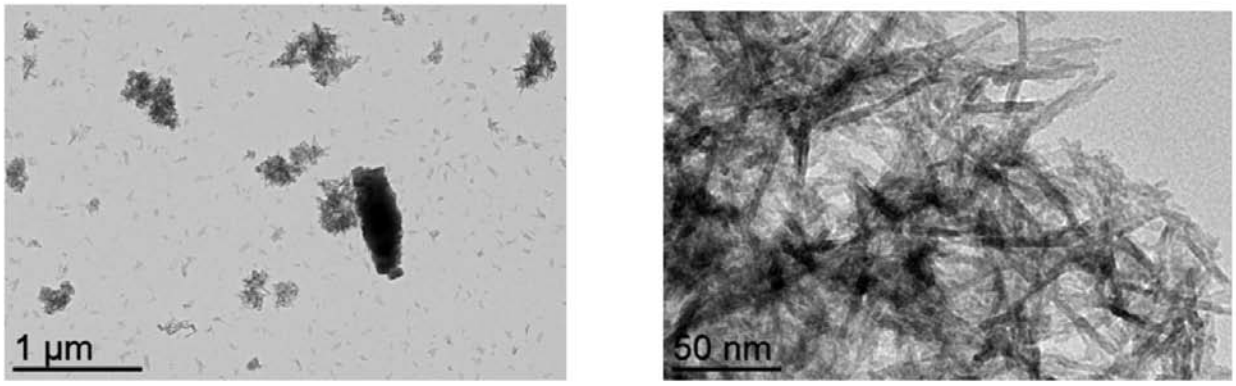

Figure 6. TEM images of hydrated alumina samples resulting from electrolysis with 0.1 mol/L Na_2SO_4.

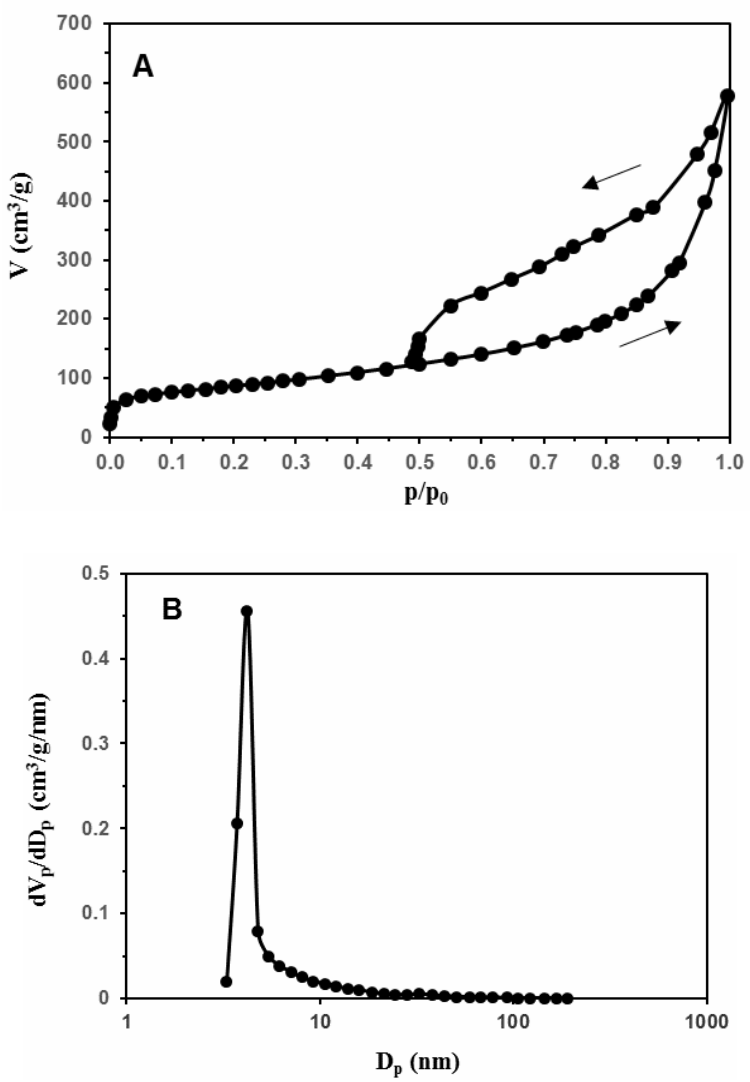

Figure 7. Nitrogen adsorption-desorption isotherm (A) and pore size distribution (B) of the boehmite sample resulting from electrolysis with 0.1 mol/L $(NH_4)_2SO_4$.

considered. In some cases, equilibrium constants and solution speciation were calculated at 60 °C, using the Phreeqc thermodynamic software [54] and the Thermoddem database [55].

During electrolysis, aluminum and water oxidations take place at the anode although aluminum oxidation is by far the major reaction. For the clarity of the discussion, water oxidation reaction was thus not considered in the following equations.

Owing to the initial pH at 9 and according to the speciation diagram of aluminum (content in molar fraction) in aqueous solution at 60 °C, see Figure 8, aluminum ions are essentially in the form of aluminate anions $Al(OH)_4^-$.

The main anodic reaction is thus expressed as:

$$Al_{(m)} + 4OH^-_{(aq)} \rightarrow Al(OH)^-_{4(aq)} + 3e^- \quad (3)$$

At the cathode, i.e. platinum plate, water reduction occurs through:

$$H_2O + 1e^- \rightarrow \frac{1}{2}H_{2(g)} + OH^-_{(aq)} \quad (4)$$

As a result, the main electrochemical reaction corresponds to:

$$Al_{(m)} + OH^-_{aq} + 3H_2O \rightarrow Al(OH)^-_{4(aq)} + \frac{3}{2}H_{2(g)} \quad (5)$$

As reported in the literature [56-59], the equilibrium solubility governing boehmite formation from aluminates is given by:

$$Al(OH)^-_{4(aq)} = AlOOH_{(s)} + H_2O + OH^-_{(aq)} \quad (6)$$

With increasing aluminate content, precipitation conditions are favourable so that AlOOH solid phase forms and accumulates. However, if pH conditions become too alkaline, aluminate anions are involved in another equilibrium solubility leading to trihydroxide phase formation through:

$$Al(OH)^-_{4(aq)} = Al(OH)_{3(s)} + OH^-_{(aq)} \quad (7)$$

The different results obtained with sodium and ammonium electrolytes are assumed to originate from electrode reactions of the electrolyte components. The acid-base equilibrium of ammonium/ammonia allows a buffering effect to take place [51]:

$$NH^+_{4(aq)} + OH^-_{(aq)} = NH_{3(aq)} + H_2O \quad (8)$$

At 60 °C, the calculated pK_a value for the ammonium/ammonia couple is 8.43. The relative

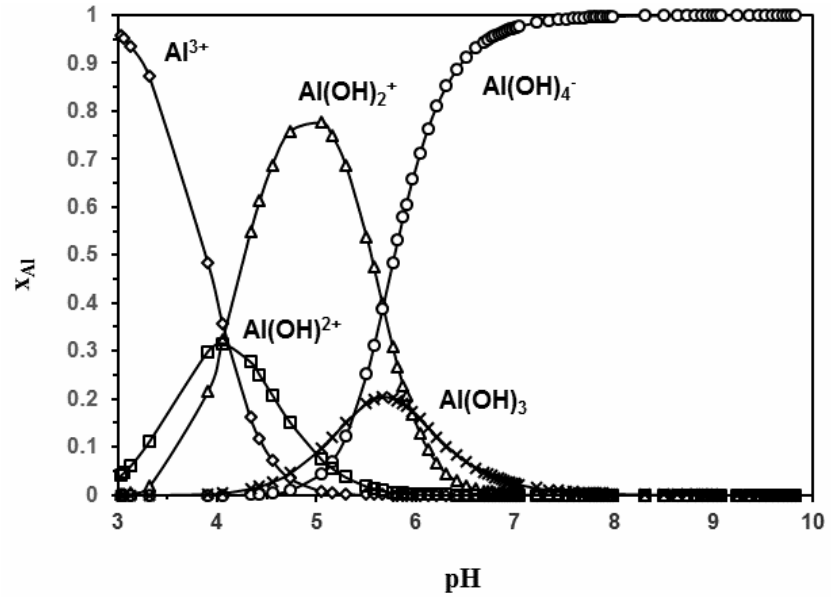

Figure 8. Calculated speciation diagram of aluminum as a function of solution pH at 60 °C, obtained with the software PHREEQC and database Thermoddem V1.10.

proportion of ammonia and ammonium in the system is then related to the pH level. Whatever their relative amount, ammonium cations and ammonia are involved in oxidation reactions, respectively, through:

$$2NH^{+}_{4(aq)} + 8OH^{-}_{(aq)} \rightarrow N_{2(g)} + 8H_2O + 6e^{-} \quad (9)$$

$$2NH_{3(aq)} + 6OH^{-}_{(aq)} \rightarrow N_{2(g)} + 6H_2O + 6e^{-} \quad (10)$$

As a consequence, hydroxyl OH^- anions are consumed and prevent a significant increase of pH during electrolysis in this case. In the presence of sodium salts, there is no such consumption of OH^- anions nor a buffering effect.

Nevertheless, sulfate anions are involved in a reduction reaction where OH^- anions are released as:

$$SO^{2-}_{4(aq)} + 5H_2O + 8e^{-} \rightarrow HS^{-}_{(aq)} + 9OH^{-}_{(aq)} \quad (11)$$

These reasons explain why pH values increase in the presence of Na_2SO_4 electrolyte, see Figure 2. When $(NH_4)_2SO_4$ is used, the released OH^- anions are compensated owing to reactions (8) and (9) and/or (10), so that pH never exceeds 9 and the exclusive formation of boehmite is guaranteed in accordance with the expected trends reported in Figure 1. Although the kinetics of these electrochemical reactions is not known, pH variation is expected to result from their competition.

To confirm the influence of pH, an additional experiment was carried out with the Na_2SO_4 electrolyte during which pH was maintained at around 9 thanks to regular additions of aliquots of concentrated H_2SO_4 solution. In these conditions, only boehmite was effectively obtained, as illustrated by XRD analysis and TEM images in Figure 9.

As reported in Table 1, EDS analysis indicates the presence of sulfur (S) atoms when $(NH_4)_2SO_4$ is used, whereas no sulfur is detected when using Na_2SO_4. This observation is ascribed to the surface properties of boehmite. As indicated, the exclusive formation of boehmite during electrolysis is conditioned to the use of ammonium salt since pH never exceeds 9. As the iep of boehmite is known to be around pH 9, it is expected that when pH < iep the boehmite surface acquires a positive charge during electrolysis owing to its amphoteric character [60] according to:

$$AlOOH_{(s)} + H^{+}_{(aq)} = AlOOH^{+}_{2(s)} \quad (12)$$

As a consequence, boehmite surface should exhibit adsorption sites for SO_4^{2-} anions through electrostatic attractions, thus justifying the detection of sulfur atoms in the corresponding boehmite sample (even after rinsing of the collected paste with water).

Anion adsorption on specific facets of boehmite crystallite causes a decrease of the surface energy of the involved facets and their growth is reduced following the Gibbs-Wulff law [61]. As reported in the literature [18, 62], the common shape of boehmite crystallite is rhombohedral with a basal facet (100) and three exposed edge facets (001), (010) and limited (101), see Figure 10.

The anisotropic structure of boehmite crystallite was assumed to result from the selective adsorption of anions on the OH-containing (010) and (001) facets, i.e. those that can act as protonated adsorption sites when pH < iep, thus explaining the preferential growth of boehmite along (100) direction. Moreover, sulfate adsorption on (010) and (001) facets inhibits aggregation of boehmite crystallites on these facets. As a result, aggregation occurs through the stacking of these nanoparticles along the (100) direction thus explaining the origin of the fibrillar aspect, and aggregation of the crystallites is enhanced since attractive van der Waals forces are dominant at such ionic strength (0.1 mol/L).

In the presence of sodium sulfate, boehmite nanofibers are produced from the beginning of electrolysis. However, when pH becomes higher than 9, i.e. when pH > iep, sulfate anions no longer adsorb onto boehmite during electrolysis and they even desorb from the surface since a negative charge is created on the surface (amphoteric character) according to:

$$AlOOH_{(s)} + OH^{-}_{(aq)} = AlOO^{-}_{(s)} + H_2O \quad (13)$$

This justifies the EDS result for the corresponding sample.

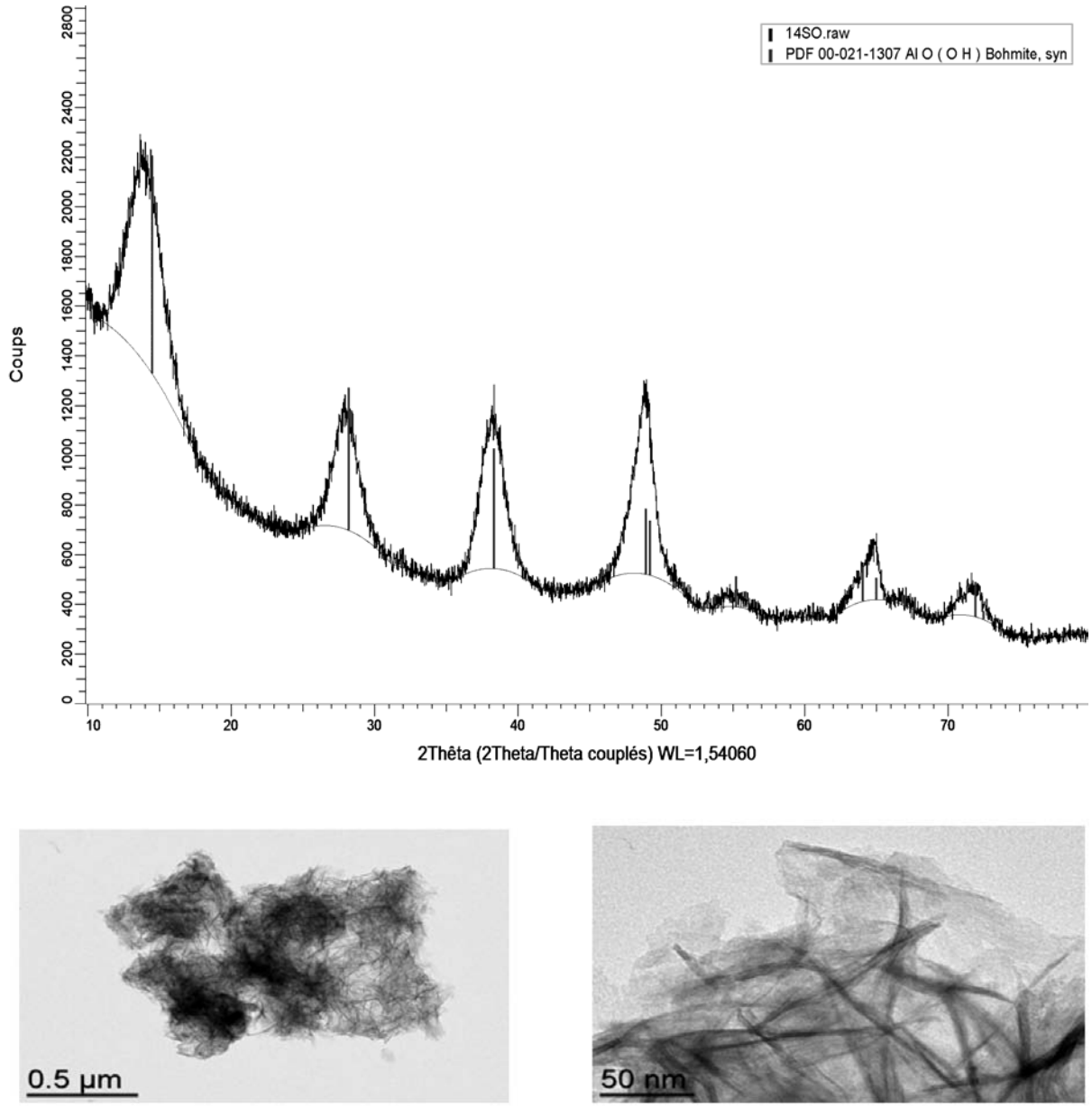

Figure 9. XRD analysis and TEM images of the boehmite sample resulting from electrolysis with 0.1 mol/L Na_2SO_4 maintained at pH around 9.

When the pH of a prepared aqueous boehmite suspension (sample obtained from electrolysis with $(NH_4)_2SO_4$ at 0.1 mol/L) was brought to 12 through addition of NaOH solution and then equilibrated during 1 hour under agitation at ambient temperature, the resulting rinsed powder exhibited a sulfur content below the detection limit of EDS analysis (< 0.1%) whereas it was initially 1.0% (see Table 1). This reflects that pure nano-fibrillar boehmite can be obtained due to the facilitated removal of adsorbed sulfate anions in alkaline media.

CONCLUSION

Although nano-fibrillar boehmite is commonly synthesized at the industrial level from precipitation reactions of aluminum salts in alkaline media at pH 9 and 60 °C, to our knowledge the present

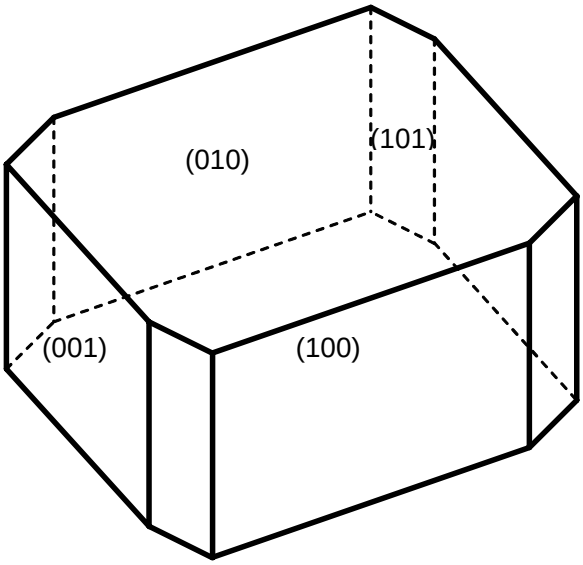

Figure 10. Schematic representation of a rhombohedric crystallite of boehmite.

work is the first study reporting its exclusive formation through electrolysis from aluminate solutions. The resulting samples were found to present the same desired properties as those from precipitation routes.

Hydrated alumina phases have been already obtained, either pure or in mixture, from electrolysis in the presence of aluminum plates but without any anticipated control. In this study, the reasons allowing to synthesize boehmite through this electrolysis process are exposed. The role of electrolyte composition in pH variation during electrolysis was shown, thereby emphasizing its influence on the resulting nature of the obtained hydrated alumina phases. As sulfates have been recognized to be important morphology-directing agents to obtain such nanomaterials, the requirement of the ammonium salt has been justified for the exclusive formation of boehmite phase through electrolysis. It has been also shown that highly purified boehmite sample can be obtained through a washing procedure in alkaline media.

In the context of sustainable development, this simple and inexpensive electrolysis process may offer the opportunity to recycle scraps or pieces of aluminum materials to produce pure nano-fibrillar boehmite samples.

ACKNOWLEGMENTS

The authors are grateful to: C. Charvillat, from the Centre Interuniversitaire de Recherche et d'Ingénierie des Matériaux (CIRIMAT Toulouse), for XRD measurements; L. Weingarten, from the Centre de Microcaractérisation Raimond Castaing (Toulouse), for TEM analysis; and M. L. De Solan-Bethmale, from the Laboratoire de Génie Chimique, for EDS analysis.

CONFLICT OF INTEREST STATEMENT

The authors declare no competing financial interest.

REFERENCES

1. Lippens, B. C. 1961, PhD Thesis, Delft University of Technology, Netherlands.
2. Wefers, K. and Misra, C. 1987, Alcoa Technical Paper N°19, Alcoa Laboratories.
3. Poisson, R., Brunelle, J. P. and Nortier, P. 1987, Catalyst Supports and Supported Catalysts, A. B. Stiles (Ed.), Butterworths, Boston, 11.
4. Euzen, P., Krokidis, X., Raybaud, P., Toulhouat, H., Le Loarer, J. L., Jolivet, J. P. and Froidefond, C. 2002, Alumina, Handbook of Porous Solids, F. Schuth, K. S. W. Sing and J. Weitkamp (Eds.), Wiley-VCH Verlag GmbH, Weinheim, Vol. 3.
5. Kirchner, S. 2015, PhD Thesis, Institut National Polytechnique de Toulouse, France.
6. Okada, K., Nagashima, T., Kameshima, Y., Yasumori, A and Tsukada, T. 2002, J. Colloid Interface Sci., 253, 308.
7. Hochepied, J. F. and Nortier, P. 2002, Powder Tech., 128, 268.
8. Hochepied, J. F., Ilioukhina, O. and Berger, M. H. 2003, Mat. Lett., 57, 2817.
9. Panias, D. and Krestou, A. 2007, Powder Tech., 175, 163.
10. Haberkorn, H., Franke, D., Frechen, T., Goesele, W. and Rieger, J. 2003, J. Colloid Interface Sci., 259, 112.
11. Kirchner, S., Teychene, S., Boualleg, M., Dandeub, A., Frances, C. and Biscans, B. 2015, Chem. Eng. J., 280, 65.
12. Bugosh, J. 1961, J. Phys. Chem., 65, 1789.
13. Brusasco, R., Gnassi, J., Tatian, C., Baglio, J., Dwight, K. and Wold, A. 1984, Mat. Res. Bull., 19, 1489.

14. Mishra, D., Anand, S., Panda, P. K. and Das, R. P. 2000, Mat. Lett., 42, 38.
15. Panda, P. K., Jaleel, V. A. and Usha Dev 2006, J. Mater. Sci., 41, 8386.
16. Chen, X. Y. and Lee, S. W. 2007, Chem. Phys. Lett., 438, 279.
17. Chen, X. Y., Zhang, Z. J., Li, X. L. and Lee, S. W. 2008, Solid St. Comm., 145, 368.
18. He, T., Xiang, L. and Zhu, S. 2008, Langmuir, 24, 8284.
19. He, T., Xiang, L. and Zhu, S. 2009, Cryst. Eng. Comm., 11, 1338.
20. Wang, X. M., Li, X. Y. and Shih, K. 2011, J. Am. Ceram. Soc., 94, 4435.
21. Song, J., Li, Z., Xu, X., He, M., Li, Z., Wang, Q. and Yan, L. 2013, Ind. Eng. Chem. Res., 52, 7752.
22. Yoldas, B. E. 1973, J. Appl. Chem. Biotechnol., 23, 803.
23. Tsukada, T., Segawa, H., Yasumori, A. and Okada, K. 1999, J. Mater. Chem., 9, 549.
24. Kuiry, S. C., Megen, E., Patil, S. D., Deshpande, S. A. and Seal, S. 2005, J. Phys. Chem. B., 109, 3869.
25. Zhu, Y., Jiang, Z., Zhang, L., Shi, J. and Yang, D. 2012, Ind. Eng. Chem. Res., 51, 255.
26. Lee, Y. P., Liu, Y. H. and Yeh, C. S. 1999, Phys. Chem. Chem., 1, 4681.
27. Shen, S. C., Chen, Q., Chow, P. S., Tan, G. H., Zeng, X. T., Wang, Z. and Tan, R. B. H. 2007, J. Phys. Chem. C, 111, 700.
28. van Straten, H. A., Holtkamp, B. T. W. and De Bruyn, P. L. 1984, J. Colloid Interface Sci., 98, 342.
29. van Straten, H. A. and De Bruyn, P. L. 1984, J. Colloid Interface Sci., 102, 260.
30. Music, S., Dragcevic, D. and Popovic, S. 1995, Mat. Lett., 24, 59.
31. Music, S., Dragcevic, D. and Popovic, S. 1999, Mat. Lett., 40, 269.
32. Du, X., Wang, Y., Su, X. and Li, J. 2009, Powder Tech., 192, 40.
33. Candela, L. and Perlmutter, D. D. 1992, Ind. Eng. Chem. Res., 31, 694.
34. Violante, A. and Violante, P. 1980, Clays Clay Miner., 28, 425.
35. Gong, X., Nie, Z., Qiou, M., Liu, J., Pederson, L. A., Hobbs, D. T. and McDuffie, N. G. 2003, Ind. Eng. Chem. Res., 42, 2163.
36. Prodromou, K. P. and Pavlatou-Ve, A. S. 1995, Clays Clay Miner., 43, 111.
37. Mishra, D., Anand, S., Panda, R. K. and Das, R. P. 2002, Mat. Lett., 53, 133.
38. Xu, X., Zhang, B. and Hu, Z. 2013, Powder Tech., 239, 272.
39. Cesteros, Y., Salagre, P., Medina, F. and Sueiras, J. E. 1999, Chem. Mater., 11, 123.
40. Rousseaux, J. M., Weisbecker, P., Muhr, H. and Plasari, E. 2002, Ind. Eng. Chem. Res., 41, 6059.
41. Zhu, H. Y., Gao, X. P., Song, D. Y., Bai, Y. Q., Ringer, S. P., Gao, Z., Xi, Y. X., Martens, W., Riches, J. D. and Frost, L. R. 2004, J. Phys. Chem. B, 108, 4245.
42. Raybaud, P., Digne, M., Iftimie, R., Wellens, W., Euzen, P. and Toulhouat, H. 2001, J. Cat., 201, 236.
43. Jolivet, J. P., Froidefond, C., Pottier, A., Chaneac, C., Cassaignon, S., Tronc, E. and Euzen, P. 2004, J. Mater. Chem., 14, 3281.
44. Chen, G. 2004, Sep. Purif. Technol., 38, 11.
45. Mansouri, K., Ibrik, K., Bensalah, N. and Abdel-Wahab, A. 2011, Ind. Eng. Chem. Res., 50, 13362.
46. De Souza Santos, P., De Freitas Neves, R. and De Souza Santos, H. 1993, Colloid Polym. Sci., 271, 197.
47. Woo, S., Lee, M. K. and Rhee, C. K. 2007, Mater. Sci. Forum, 534, 129.
48. Flilissa, A., Meleard, P. and Darchen, A. 2013, Water Treat., 51, 6719.
49. Tchomgui-Kamga, E., Audebrand, N. and Darchen, A. 2013, J. Haz. Mat., 254, 125.
50. Trompette, J. L., Vergnes, H. and Coufort, C. 2008, Coll. Surf. A, 315, 66.
51. Trompette, J. L. and Vergnes, H. 2009, J. Haz. Mat., 163, 1282.
52. Wood, R., Fornasiero, D. and Ralston, J. 1990, Colloids Surf., 51, 389.
53. Hiementz, P. C. 1986, Principles of Colloid and Surface Chemistry, 2nd Ed., Dekker, New York.
54. Parkhurst, D. L. and Appelo, C. A. J., Geological Survey Techniques and Methods, Book 6, Chap. A43, p. 497.
55. Blanc, P., Lassin, A., Piantone, P., Azaroual, M., Jacquemet, N., Fabbri, A. and Gaucher, E. C. 2012, Appl. Geochem., 27, 2107.

56. Chang, B. T. 1981, Bull. Chem. Soc. Jpn., 54, 2579.
57. Verdes, G., Gout, R. and Castet, S. 1992, Eur. J. Miner., 4, 767.
58. Apps, J. A., Neil, J. M. and Jun, C. H. 1988, Earth Sciences Division, LBL-21482, Berkeley.
59. Benezeth, P., Palmer, D. A. and Wesolowski, D. J. 2001, Geochim. Cosmochim. Acta, 65, 2097.
60. Franks, G. V. and Gan, Y. 2007, J. Am. Ceram. Soc., 90, 3373.
61. Jolivet, J. P., Chaneac, C., Chiche, D., Cassaignon, S., Durupthy, O. and Hernandez, J. 2011, C. R. Geosciences, 343, 113.
62. Karouia, F., Boualleg, M., Digne, M. and Alphonse, P. 2013, Powder Tech., 237, 602.